Angewandte Chemie
International Edition

Accepted Article

Authors: Qi Yin, Eugeny V. Alexandrov, Duan-Hui Si, Qian-Qian Huang, Zhi-Bin Fang, Yuan Zhang, An-An Zhang, Wei-Kang Qin, Yu-Lin Li, Tian-Fu Liu, and Davide M. Proserpio

WILEY-VCH

RESEARCH ARTICLE

Metallization-Prompted Robust Porphyrin-Based Hydrogen-Bonded Organic Frameworks for Photocatalytic CO₂ Reduction

Qi Yin,[a] Eugeny V. Alexandrov,[c],[e] Duan-Hui Si,[a] Qian-Qian Huang,[a] Zhi-Bin Fang,[a] Yuan Zhang,[a] An-An Zhang,[a] Wei-Kang Qin,[a],[d] Yu-Lin Li,[a],[d] Tian-Fu Liu*,[a],[d] and Davide M. Proserpio[b],[c]

[a]   Q. Yin, D. Si, Q. Huang, Z. Fang, Y. Zhang, A. Zhang, W. Qin, Y. Li, and T. Liu
      State Key Laboratory of Structural Chemistry
      Fujian Institute of Research on the Structure of Matter, Chinese Academy of Sciences
      350002, Fuzhou, Fujian, P. R. China
      Email: tfliu@fjirsm.ac.cn
[b]   D. M. Proserpio
      Universita degli studi di Milano
      Dipartimento di Chimica
      20133 Milano, Italy
[c]   E. V. Alexandrov and D. M. Proserpio
      Samara Center for Theoretical Material Science (SCTMS), Samara State Technical University, Samara 443100, Russia.
      Samara Center for Theoretical Material Science (SCTMS)
      Samara State Technical University
      443100, Samara, Russia
[d]   W. Qin, and T. Liu
      University of Chinese Academy of Sciences, No.19 (A) Yuquan Road, Shijingshan District, Beijing, 100049, P. R. China
      University of Chinese Academy of Sciences
      100049, No.19 (A) Yuquan Road, Shijingshan District, Beijing, P. R. China
[e]   E. V. Alexandrov
      Institute of Experimental Medicine and Biotechnology
      Samara State Medical University
      443099 Samara, Russia

      Supporting information for this article is given via a link at the end of the document.

Abstract: Under the topological guidance, the self-assembly process based on tetratopic porphyrin synthon results in a HOF with the predicted square layers topology (sql) but unsatisfied stability. Strikingly, simply introducing transition metal in porphyrin center does not change the network topology but drastically causes noticeable change on noncovalent interaction, orbital overlap, and molecular geometry, therefore ultimately giving rise to a series of metalloporphyrinic HOFs with high surface area, and excellent stability (intact after being soaked in boiling water, concentrated HCl, and heated in 270 ºC). With integrating both photosensitizers and catalytic sites into robust backbones, this series of HOFs can effectively catalyze the photoreduction of CO₂ to CO, and their catalytic performances greatly depend on the chelated metal species in porphyrin centers. This work enriches the library of stable functional HOFs and expands their applications in photocatalytic CO₂ reduction.

Introduction

Hydrogen-bonded organic frameworks (HOFs), self-assembled by organic building blocks through hydrogen bonding and weak intermolecular interactions, is a burgeoning class of crystalline porous organic materials featured with high surface area, tunable pore size and diverse functionality[1]. Moreover, the nature of hydrogen bonds endow HOFs unique traits of mild synthetic conditions[2], solution processability[3], recyclability[4], showing promising potentials for gas storage and separation[5], proton conduction[6], luminescence[7], molecular recognition[8], and so on[9].

Although emerging from as early as the 1990s, the development of HOFs is still in the early stage, which is heavily restricted by their poor stability[3]. In our previous report, we have proposed some beneficial strategies for HOF construction and verified the significance of π-conjugation for the stability of HOFs[2]. With this information, it's easy to imagine that the large π-conjugated porphyrinic moieties are promising building blocks for the self-assembly of stable HOFs, which, in the meantime, endows material with diverse functionality due to their excellent photophysical, photochemical, and electrochemical properties etc[10]. Although many attempts have been made to synthesize porphyrinic HOFs in both our lab and others[11], high surface area, large pore size, and excellent robustness have yet to be achieved before this work. The weak intermolecular interaction, bringing in many unique physical and chemical features though, poses the challenge of controllable self-assembly and structural stability.

While in a careful search for porphyrinic HOFs and supramolecular organic frameworks (known as SOFs), we found the reported porphyrinic structure are either out of the topology guidance (dense packing without accessible cavities) or with the aromatic macrocycles far away from each other in the absence of strong π-π stacking interactions (resulting in low structural stability)[12]. To simultaneously achieve high porosity and framework robustness, we are seeking to find other dominant factors affecting the self-assembled results [13]. In homogenous porphyrin system, the metalloporphyrin center has been considered as one of the most important factors determining the robustness and activity of materials. Varying the metal centers causes the dramatic changes of electronic structures of macrocyclic rings, axial bonding/interaction, and the geometry of peripheral substitution[14]. Specifically, it has been proven that the

RESEARCH ARTICLE

metal center would influence the extent of through-ligand orbital overlap (conjugation) as well as weak interactions of peripheral groups.[15] Therefore, we can anticipate that porphyrinic building blocks with different metal centers may greatly influence the self-assembled results and the stability of HOFs.

With this consideration, we started from tetratopic carboxylate porphyrin ligand and carefully tuned the synthetic condition to get a HOF (named as PFC-71) with square layer (**sql**) network under topology guidance. The adjacent porphyrin centers in PFC-71 are far away from each other and therefore exhibit comparatively low structural stability. Metallizing the porphyrin centers give rise to identical network but larger orbital overlap between interlamellar porphyrin cores (named as PFC-72 and PFC-73 series, Figure 1), therefore enormously improving their structural stability. This series of HOFs exhibit high surface area, excellent thermal and chemical stability (intact upon heated in 270 °C, maintaining crystallinity in concentrated HCl for 1 day). Besides, the thermal destroyed PFC-73-Ni/Cu can be readily recovered through simple acid or solvent treatments. Meanwhile, in consideration of the ordered integration of porphyrinic photosensitizers and metal cores as potential catalytic sites, photocatalytic CO_2 reduction without additional photosensitizers and co-catalysts is adopted to evaluate the influence of diffrenent metalloporphyrin on the catalytic activities. Among them, cobalt porphyrinic HOF shows the optimal performance for the conversion of CO_2 to CO.

Results and Discussion
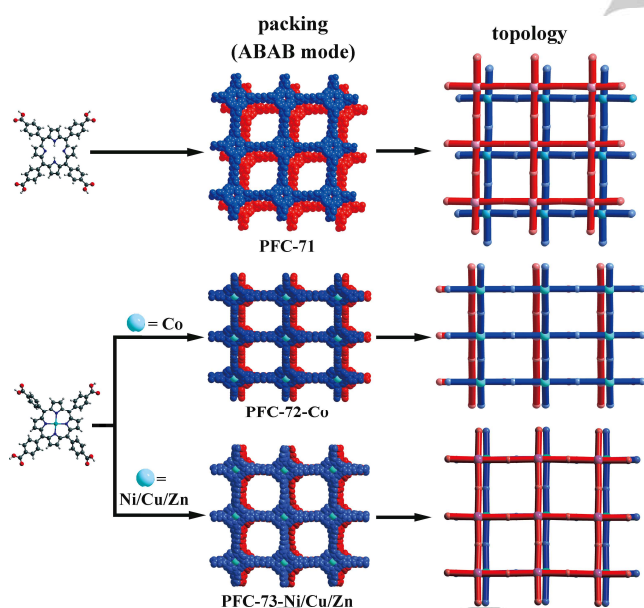
Figure 1. Schematic representation of the construction of PFC-71, PFC-72-Co, and PFC-73-Ni/Cu/Zn.

[5,10,15,20-Tetrakis(4-carboxyphenyl)porphyrin] (TCPP) or [5,10,15,20-Tetrakis(4-carboxyphenyl)porphrin]-M (TCPP-M, M=Co, Ni, Cu, Zn) ligand was dissolved in a mixture of N,N-dimethylformamide (DMF) and 1,2,4-Trichlorobenzene (TCB). The mixture was exposed and held at 100 °C or 130 °C for 2 days to yield crystals suitable for x-ray determination. The powdery samples were synthesized at 100 °C in a similar way. Besides,

the powdery PFC-71 to PFC-73 materials with good crystallinity can also be obtained through holding the solution of TCPP/TCPP-M (M=Co/Ni/Cu/Zn) ligands in CH_3COOH at 90 °C for 2 days (more details in supporting information). Note that, PFC-73-Ni/Cu/Zn have identical crystal structure, topology, and packing mode, only differ from each other in the central metal species (Figure 1).

Table 1. Structural Parameters of PFC-71, PFC-72-Co, and PFC-73-Cu.

|	PFC-71	PFC-72-Co	PFC-73-Cu
Ligand	TCPP	TCPP-Co	TCPP-Cu
O-H···O distance (Å)	2.58 2.64	2.63 2.88	2.57 2.61 2.62 2.64
Layer thickness (Å)	6.26	7.62	6.64
Interlayer distance (Å)	3.94	3.62	3.82
Interlamellar porphyrin center-to-center distance (Å)	7.30	5.44	5.08
Pore size (Å)	14.9 x 14.9	15.7 x 18.6	18.0x18.8
Accessible volumea	60.2%	53.6%	52.8%
BET surface area (m2/g)	600	1646	1714 1720 for M=Ni 1856 for M=Zn

a Calculated by PLATON software.

Single crystal X-ray diffraction revealed that PFC-71 crystallized in monoclinic system with C2/c space group. Each porphyrin ligand interacts with four neighboring ones through eight O–H···O hydrogen bonds to extend into a two-dimensional (2D) square layer. All hydrogen bonds (O-H···O) in the three structures are in the range 2.57-2.88 and could be classified as moderate [16]. Adjacent layers are stacking as ABAB along c-axis to form one-dimensional channels about 14.9 ×14.9 Å^2 (Figure 2a-2b, S9). Insertion of metal cation into porphyrin ring deforms the shape of TCPP into more non-flat saddle-like geometry (Figure S38, Table S3). Meanwhile, the interlamellar porphyrin center-to-center distances in PFC-72-Co and PFC-73-M (M = Ni, Cu, Zn) were dramatically shortened (5.44 Å and 5.08 Å, respectively) compared with that in the metal-free PFC-71 (7.30 Å, Table 1, Figure 2c-2e, S3-5), which caused much larger interlayer orbital overlap, stronger π-π interactions, and short metal-carbon VdW interactions (<3.6 Å) (Figure 2f-2h, S38-40, Table S4). Simultaneously, it is observed an increase of the intermolecular contact area measured from the faces of molecular Voronoi polyhedra[17] for the molecule interacting from neighboring layers. The original self-assembly mode (the packing remains ABAB) does not change (Figure S1-S2). However, more intermolecular interactions shorten the interlayer distance and increases the overlap between layers and the density of crystals. Accompanied with the variation on space group and the size of square channels, PFC-72-Co crystallized in P2/c space group with an opening about 18.6 × 15.7 Å^2, and PFC-73-M crystallize in P2$_1$/c with an opening about 18.8 × 18.0 Å^2 (Figure S10-11). The size of channels enlarges in the metallized structures because of the aligning of flat 4-carboxyphenyl groups along channel, and the

2

channel surface becomes less corrugated. In the structure of PFC-71, large 1D channels communicate to each other through narrow windows with an opening about 3.4 × 8.3 Å (Figure S9b). Due to denser packing and different alignment of 4-carboxyphenyl groups, such windows disappear in PFC-72-Co and PFC-73-M, causing the decreased theoretical accessible surface area from 2078 m^2/cm^3 (PFC-71) down to 1292 m^2/cm^3 (PFC-72-Co) and 1280 m^2/cm^3 (PFC-73-Cu).

The phase purities of PFC-71 to PFC-73 are confirmed by the good consistency between experimental powdery X-ray diffraction (PXRD) patterns and the simulated ones from single crystal diffraction data (Figure 3a-3e). The permanent porosity of these five HOFs are confirmed by N_2 sorption isotherms at 77 K, which all show type I isotherms representative of microporous materials (Figure 3f). Although the as-synthesized (solvated) PFC-71 shows excellent crystallinity suitable for single-crystal x-ray analysis, framework partially collapses upon activation even at very mild conditions at 65 °C due to the relative low stability. Therefore, activated PFC-71 shows much lower N_2 uptake (160 cm^3/g), Brunauer−Emmett−Teller (BET) surface area (600 m^2/g), and pore volumes (0.248 cm^3/g) than theoretical ones (surface

area of 3073 m^2/g and pore volume of 0.868 cm^3/g, calculated by zeo++ software[18]). Further temperature rise results in worse crystallinity and much decreased BET surface area[19] (Figure S13). The narrow windows (about 4.3 Å) seen from theoretical calculations is absent in the plot of experimental pore size distribution (Figure S9b). In contrast, metalloporphyrin-based HOFs exhibit much larger BET surface area (and pore volume): 1646 m^2/g (0.683 cm^3/g) for PFC-72-Co, 1856 m^2/g (0.748 cm^3/g) for PFC-73-Zn, 1714 m^2/g (0.692 cm^3/g) for PFC-73-Cu, and 1720 m^2/g (0.706 cm^3/g) for PFC-73-Ni (Figure S31, S33, S35, S37), which are closer to the simulated results of 1630 m^2/g (0.665 cm^3/g) for PFC-72-Co and 1700 m^2/g (0.747 cm^3/g) for PFC-73-Cu. Of special note, these HOFs show high N_2 saturated uptake and excellent surface area among reported HOFs (Table S2). Besides, non-local density functional theory (NLDFT) pore size distributions of PFC-71 to PFC-73 matched with their corresponding calculated value deduced from crystal structures (Figure S28, S30, S32, S34, Table S3).
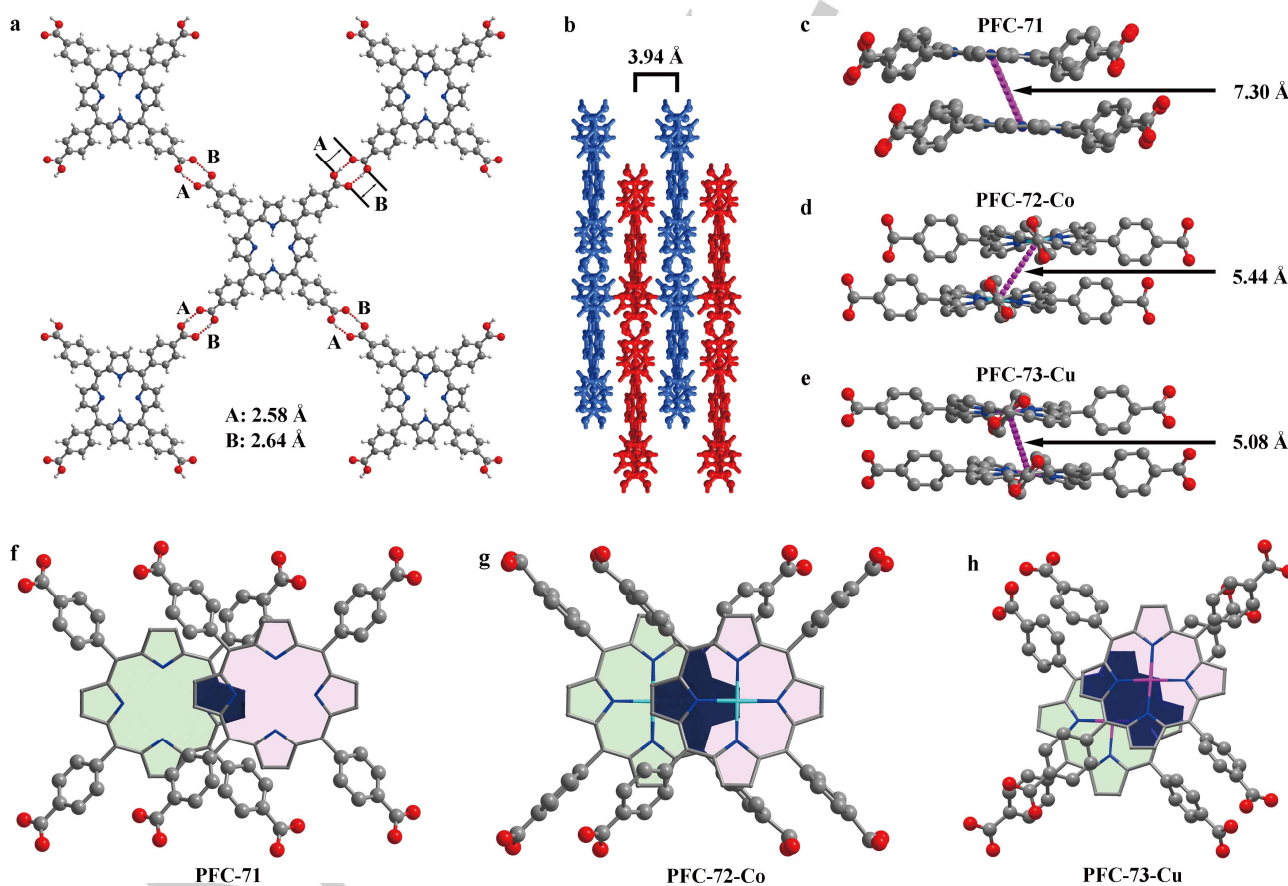
Figure 2. a) View of PFC-71 structure and the connection of adjacent building blocks with two kinds of hydrogen bonds (A: 2.58 Å, B: 2.64 Å). b) The ABAB stacking mode of PFC-71 showing interlayer distance of 3.94 Å. c) The offset π-π interactions of PFC-71 viewed from (010) plane (c) and (-101) plane (f), PFC-72-Co from (010) plane (d) and (101) plane (g), and PFC-73-Cu from (010) plane (e) and (001) plane (h), showing interlayer porphyrin center-to-center distance and orbital overlap area highlighted with dark blue (hydrogen atoms are omitted for clarity).

3

10.1002/anie.202115854

WILEY-VCH

RESEARCH ARTICLE
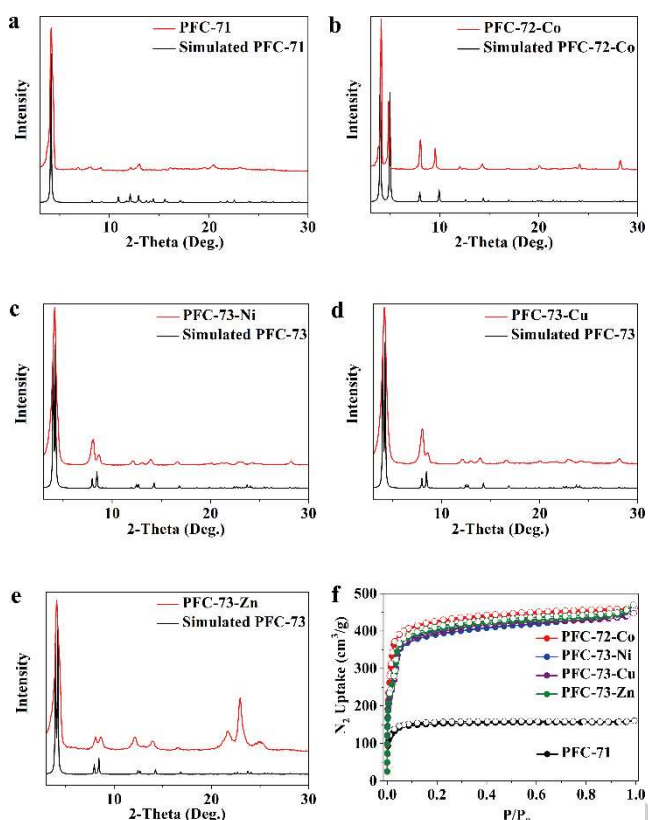
Figure 3. Experimental and simulated PXRD patterns for (a) PFC-71, (b) PFC-72-Co, (c) PFC-73-Ni, (d) PFC-73-Cu, and (e) PFC-73-Zn; f) N_2 sorption isotherms (77 K) of PFC-71 to PFC-73.

PFC-71 exhibits much lower structural stability than PFC-72 and 73. Heating at 120 °C and 150 °C for 6 hours severally reduces the N_2 uptake of PFC-71 from 160 cm^3/g to 112 cm^3/g and 65 cm^3/g, respectively (Figure 4a, S13), and treating PFC-71 with water causes significant structure collapse. In contrast, metallization of porphyrin center endows HOFs with much improved robustness (Figure 4b-e). Taking PFC-73-Cu as an example, PXRD patterns demonstrate that PFC-73-Cu can maintain crystallinity after being soaked in MeOH, EtOH, Acetone, CH_2Cl_2, $CHCl_3$, CH_3CN, water, pH 10 aqueous solution, and concentrated HCl for 1 day (Figure S22-23), showing a wide range of chemical stability. Of special note, PFC-73-Cu can even survive boiling water for 1 day. Besides the dramatically improved robustness, metalloporphyrin building blocks endow materials with strikingly acidic-assisted crystalline redemption (named as "AACR") as discovered in our previously reported HOF[2]. As shown in Figure S14, N_2 uptake of PFC-73-Cu decreased from 426 cm^3/g to 68 cm^3/g after being heated at 270 °C for 6 hours. Notably, after immersing the deteriorated samples in 0.1 M HCl aqueous solutions for 1 day, the gas uptake was recovered to 431

cm^3/g, which is nearly identical to the corresponding pristine sample. The crystalline recovery can also be achieved through immersing destroyed sample in CH_2Cl_2, named as solvent-assisted crystalline redemption (SACR) (Figure S14). Similar phenomena can be observed for metalloporphyrinic HOF PFC-73-Ni (Figure S15, S25-26). We hypothesize that the hydrogen bonds were destroyed accompanied with the carboxylic acid deprotonating during the heating process, while the addition of proton causes re-association of hydrogen bonds and therefore recovers the crystallinity of materials[2]. In sharp contrast, PFC-71 is unstable in water and cannot be regenerated through AACR process. Experimental results clearly demonstrate that metallization of the porphyrin center of HOFs is a very effective strategy to regulate the thermal/hydrolytic/chemical stability of materials. We infer this phenomenon can be ascribed to the following three factors. Firstly, the electronegativities of N atom, metal ions, and H atom follow the trend of 3.066 N > 2.30 H > 1.88 Ni, 1.84 Co, 1.85 Cu > 1.588 Zn based on the Allen scale[20]. A larger electronegativity means a stronger attraction toward electrons. With this conceptual basis, we can infer that replacing H with metal ions in porphyrin center will bring in a larger electronegativity difference on the macrocycle backbone and therefore cause increased polarizability and electron cloud distortion. In this case, the organic framework would possess more electron clouds and form stronger offset π-π interactions toward adjacent interlamellar porphyrins. Besides, as shown in Figure 2f-h and S39-41, PFC-72 and PFC-73 have much larger π-orbitals overlap area than that of PFC-71 and short metal carbon vdW interactions. Considering that the vdW forces are proportional to the contact area, PFC-72 and PFC-73 should have larger vdW forces than PFC-71. The third reason is the undulated geometry of metallized layers. The crystal structures are prone to collapse because of the sliding molecules from the H-bonded layer into the pore[21]. The deeper interlayer penetrations (overlaps) and orientation of four benzene rings orthogonal to the layer significantly increase the geometrical barrier for sliding. All these factors account for the higher stability of PFC-72 and PFC-73 over PFC-71.

To further decode how the metallization of porphyrin affects the robustness, Density functional theory (DFT) calculations were conducted to gain insights into noncovalent interactions (NCI) in structures of PFC-71 and PFC-73-Cu. NCI in fragments of both two structures can be split into in-plane hydrogen bonding interactions and interlayer binding interactions. This approach has proved its applicability in study of crystal structure stability[22]. As shown in Figure 5e, PFC-71 and PFC-73-Cu have similar in-plane binding energy (85.0 kcal/mol for PFC-71, and 81.9 kcal/mol for PFC-73-Cu), which match with their approximate hydrogen bond length. As for interlayer binding energy, the value of PFC-73-Cu (160.8 kcal/mol) is 2.1 fold higher than that of PFC-71 (76.5 kcal/mol) calculated by Gaussian program[23] (computational model in Figure S47-48). This order was also confirmed by the interaction energy
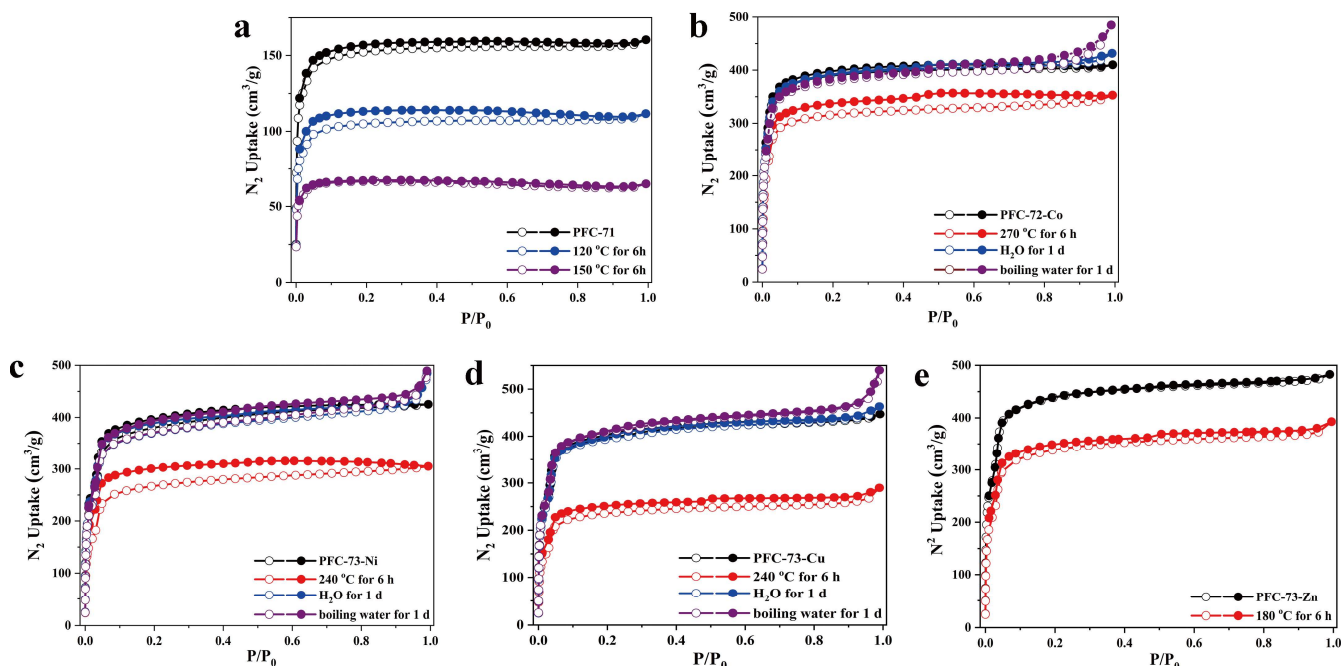
4

Figure 4. N_2 sorption isotherms (77 K) of a) PFC-71; b) PFC-72-Co; c) PFC-73-Ni; d) PFC-73-Cu; e) PFC-73-Zn after different treatments.

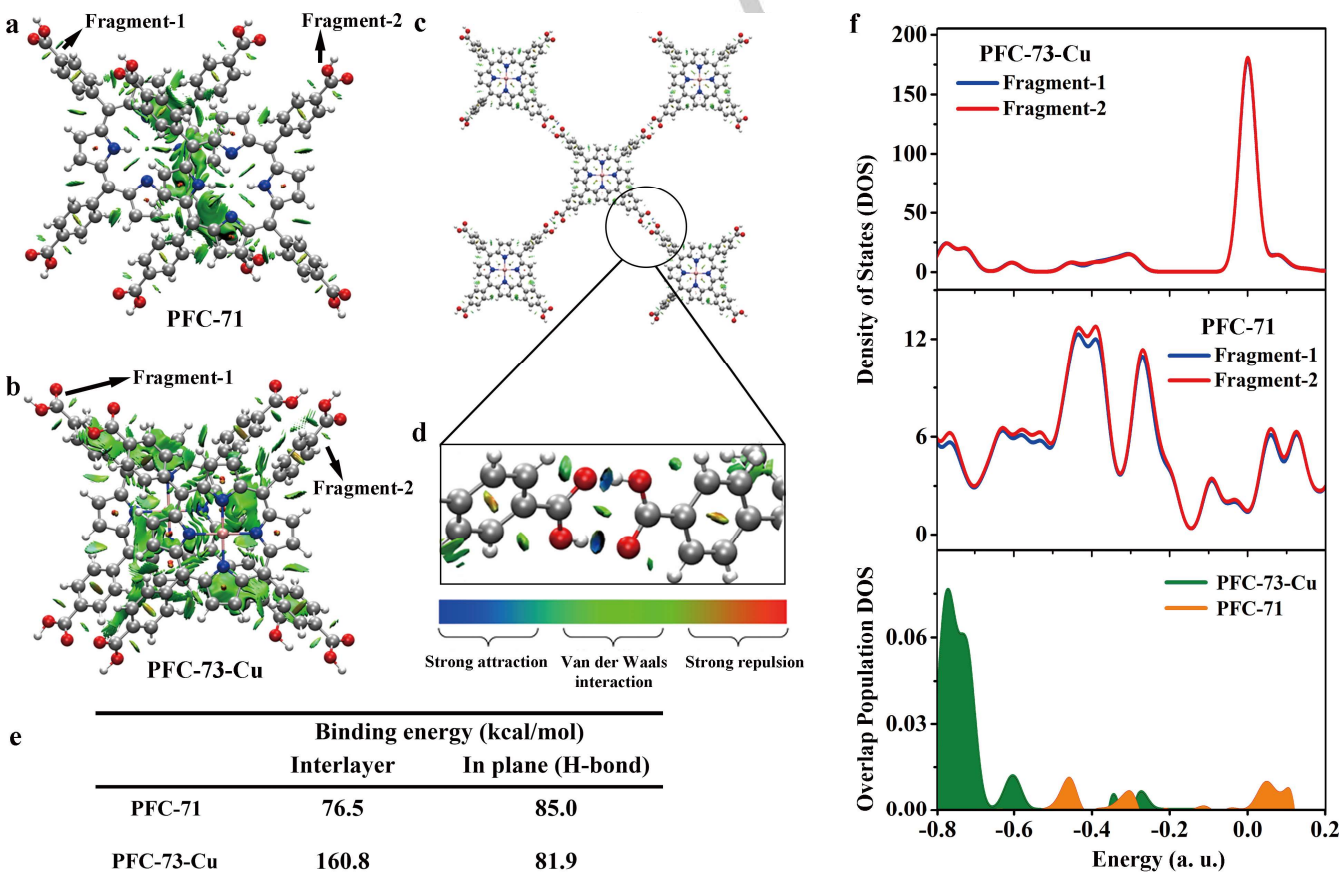|	Binding energy (kcal/mol)	
	Interlayer	In plane (H-bond)
PFC-71	76.5	85.0
PFC-73-Cu	160.8	81.9

Figure 5. Interlayer NCI isosurfaces for a) PFC-71 dimer and b) PFC-73-Cu dimer, showing the larger overlap area of PFC-73-Cu than PFC-71; c), d) PFC-71 and PFC-73-Cu show similar in-plane NCI isosurfaces with strong hydrogen bond interaction (only PFC-73-Cu was depicted as a representative); e) Calculated binding energy of PFC-71 and PFC-73-Cu; f) Comparison of DOS and the corresponding OPDOS of PFC-71 and PFC-73-Co dimer (fragment 1-2 were shown in 5a-5b).

RESEARCH ARTICLE

calculations using CrystalExplorer[24] (Figure S42-43). Based on above results, we can conclude that interlayer binding interactions are vital to the great improvement on framework robustness. To further validate our presumption, we then turn to NCI isosurfaces, electrostatic potential (ESP), and overlap distribution between interlayer porphyrin fragments from the density-of-states (DOS) and overlap population density-of-states (OPDOS) in both two HOFs. As real-space visualization of both attractive and repulsive interactions in structure based on electron density[25], NCI isosurface illustrates that PFC-71 and PFC-73-Cu have similar and strong hydrogen bonds in plane but weaker interlayer attractive interactions of former than later (Figure 5a-5d, S46). Meanwhile, PFC-71 and PFC-73-Cu also have high DOS overlap between two interlayer fragments, while the latter has higher DOS value and larger OPDOS area in bonding region (value > 0) than the former, demonstrating higher interlayer interactions of PFC-73-Cu than that of PFC-71 (Figure 5f, computational model in Figure 5a-5b). Besides, based on ESP analysis, PFC-71 and PFC-73-Cu have similar and strong bonding mode in plane to form hydrogen bonds. However, it can be found that introduction of Cu causes more electron density distortion in the porphyrin core of PFC-73-Cu than that of PFC-71 (Figure S44-45), which is also evidenced by the increase of dipole moment from 0.0449 Debye (PFC-71, out of plane) to 4.9911 Debye (PFC-73-Cu, out of plane) (Table S5). Meanwhile, the larger overlap area and the better match of negative/positive potential area in interlayer porphyrin cores are also conducive to structure stability. In summary, theoretical study reveals that metallization of porphyrin greatly changes the electrostatic potential, the density of state, and therefore the noncovalent interactions between interlayer porphyrin fragments, giving rise to a robust framework.
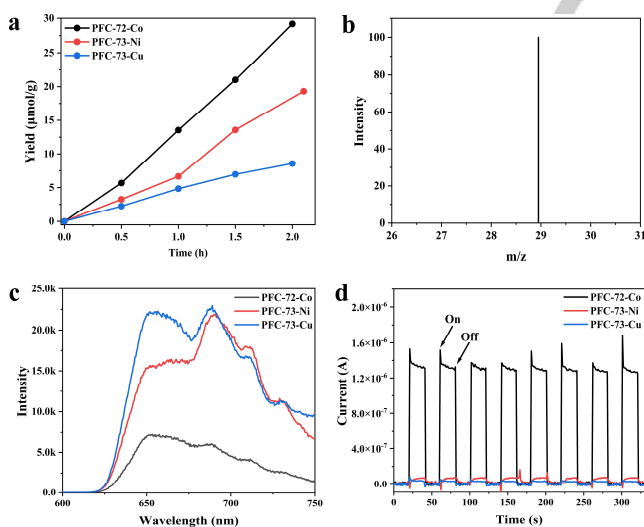
Figure 6. a) Time-resolved CO productions of photocatalytic CO_2 reduction over PFC-72-Co, PFC-73-Ni and PFC-73-Cu; b) Mass spectrum of produced ^{13}CO via isotope $^{13}CO_2$ reduction under visible light; c) Solid-state photoluminescence spectra excited at 422 nm and d) Transient photocurrent response of PFC-72-Co, PFC-73-Ni, and PFC-73-Cu.

Considering the periodic integration of porphyrinic photosensitizers and metal cores as potential catalytic sites in frameworks, three HOFs (PFC-72-Co and PFC-73-Ni/Cu) were chosen to perform photocatalytic CO_2 reduction experiments in a gas-solid regime without using additional photosensitizers and co-

catalysts. The UV-vis spectra show broad and strong absorption in the region of 200−800 nm (Figure S49), which indicates the potential photo-response properties of these materials. CO was determined as the only product of the reaction by gas chromatography and ion chromatography. Among them, PFC-72-Co emerges optimal performance (14.7 μmol/g/h), which is 1.5 fold higher than PFC-73-Ni (9.8 μmol/g/h) and 3 fold higher than PFC-73-Cu (4.4 μmol/g/h) (Figure 6a, S50). Then the ^{13}C isotope labeling experiment over PFC-72-Co suggests that CO_2 feed gas is the carbon source of the produced CO (Figure 6b and S51).

To further reveal the influence of different metalloporphyrins on the catalytic activities, conduction-band positions were firstly estimated by measuring the flat band potential (E_{fb}) based on Mott−Schottky measurements. The positive slopes suggest the characteristics of typical n-type semiconductors. And the E_{fb} are ~ −0.79 V for PFC-72-Co, ~ −0.68 V for PFC-73-Ni, and ~ −0.45 V for PFC-73-Cu, respectively, vs Ag/AgCl, which means PFC-72-Co has the highest reducing capacity (Figure S52). Meanwhile, photoluminescence (PL) spectrum indicated that, all three HOFs show emission bands at about 650 nm with successively decreased intensities for PFC-73-Cu, PFC-73-Ni, and PFC-72-Co. Together with the photocurrent response (Figure 6d) and electrochemical impedance spectra (EIS) (Figure S53), we can infer that PFC-72-Co has the most effective charge transfer and separation efficiency during the photocatalytic reaction. These results are in agreement with their CO_2 photoreduction activity and explain the reasons for the optimal performance of PFC-72-Co.

Conclusion

In summary, a series of robust porphyrin-based HOFs were designed and synthesized, resulting in three structures with the same topology but different packing modes. The metal-free porphyrinic PFC-71 has low surface area and poor stability, while the metallization of porphyrin centers endows PFC-72 and PFC-73 with high surface area and remarkable thermal, chemical and water stability, as well as easy recovery property. Crystal structure reveals that the metallization of porphyrin core drastically changes the π-π stacking and therefore the noncovalent interactions between interlayer adjacent porphyrin rings. Theoretical studies further elucidate this change from electronic structure and orbital overlap aspect. Besides the robustness, metallization of porphyrin center endows frameworks with different catalytic activities toward CO_2 photoreduction, among which PFC-72-Co shows the optimal performance. Our building strategy and findings guide and facilitate the construction of stable functional HOF materials, which not only enrich the structural diversity but broaden the application horizon of HOF materials.

RESEARCH ARTICLE

[1] a) J. Lu, R. Cao, *Angew. Chem. Int. Ed.* **2016**, *55*, 9474-9480; b) J. Tian, H. Wang, D.-W. Zhang, Y. Liu, Z.-T. Li, *Natl. Sci. Rev.* **2017**, *4*, 426-436; c) I. Hisaki, C. Xin, K. Takahashi, T. Nakamura, *Angew. Chem. Int. Ed.* **2019**, *58*, 11160-11170.

[2] Q. Yin, P. Zhao, R. J. Sa, G. C. Chen, J. Lu, T. F. Liu, R. Cao, *Angew. Chem. Int. Ed.* **2018**, *57*, 7691-7696.

[3] J. Yang, J. Wang, B. Hou, X. Huang, T. Wang, Y. Bao, H. Hao, *Chem. Eng. J.* **2020**, *399*, 125873.

[4] a) K. Ma, P. Li, J. H. Xin, Y. Chen, Z. Chen, S. Goswami, X. Liu, S. Kato, H. Chen, X. Zhang, J. Bai, M. C. Wasson, R. R. Maldonado, R. Q. Snurr, O. K. Farha, *Cell Rep. Phys. Sci.* **2020**, *1*, 100024; b) F. Hu, C. Liu, M. Wu, J. Pang, F. Jiang, D. Yuan, M. Hong, *Angew. Chem. Int. Ed.* **2017**, *56*, 2101-2104.

[5] a) J. Lu, C. Perez-Krap, M. Suyetin, N. H. Alsmail, Y. Yan, S. Yang, W. Lewis, E. Bichoutskaia, C. C. Tang, A. J. Blake, R. Cao, M. Schroder, *J. Am. Chem. Soc.* **2014**, *136*, 12828-12831; b) S. Feng, Y. Shang, Z. Wang, Z. Kang, R. Wang, J. Jiang, L. Fan, W. Fan, Z. Liu, G. Kong, Y. Feng, S. Hu, H. Guo, D. Sun, *Angew. Chem. Int. Ed.* **2020**, *59*, 3840-3845; c) Y. Liu, J. Dai, L. Guo, Z. Zhang, Y. Yang, Q. Yang, Q. Ren, Z. Bao, *CCS Chem.* **2021**, *3*, 1028-1035.

[6] A. Karmakar, R. Illathvalappil, B. Anothumakkool, A. Sen, P. Samanta, A. V. Desai, S. Kurungot, S. K. Ghosh, *Angew. Chem. Int. Ed.* **2016**, *55*, 10667-10671.

[7] a) Q. Huang, W. Li, Z. Mao, L. Qu, Y. Li, H. Zhang, T. Yu, Z. Yang, J. Zhao, Y. Zhang, M. P. Aldred, Z. Chi, *Nat. Commun.* **2019**, *10*, 3074-3081; b) Q. Huang, W. Li, Z. Yang, J. Zhao, Y. Li, Z. Mao, Z. Yang, S. Liu, Y. Zhang, Z. Chi, *CCS Chem.* **2021**, 1499-1509.

[8] C. Chen, Z. Di, H. Li, J. Liu, M. Wu, M. Hong, *CCS Chem.* **2021**, *3*, 1352-1362.

[9] a) J. F. Feng, T. F. Liu, R. Cao, *Angew. Chem. Int. Ed.* **2020**, *59*, 22392-22396; b) M. R. di Nunzio, I. Hisaki, A. Douhal, *J. Photochem. Photobiol., C* **2021**, *47*, 100418; c) B. Wang, R. He, L. H. Xie, Z. J. Lin, X. Zhang, J. Wang, H. Huang, Z. Zhang, K. S. Schanze, J. Zhang, S. Xiang, B. Chen, *J. Am. Chem. Soc.* **2020**, *142*, 12478-12485; d) B. Han, H. Wang, C. Wang, H. Wu, W. Zhou, B. Chen, J. Jiang, *J. Am. Chem. Soc.* **2019**, *141*, 8737-8740; e) W. Liang, F. Carraro, M. B. Solomon, S. G. Bell, H. Amenitsch, C. J. Sumby, N. G. White, P. Falcaro, C. J. Doonan, *J. Am. Chem. Soc.* **2019**, *141*, 14298-14305.

[10] a) C. A. Hunter, J. K. M. Sanders, *J. Am. Chem. Soc.* **1990**, *112*, 5525-5534; b) Y. Chen, A. Li, Z. H. Huang, L. N. Wang, F. Kang, *Nanomaterials* **2016**, *6*, 51-67.

[11] Q. Yin, J. Lü, H.-F. Li, T.-F. Liu, R. Cao, *Cryst. Growth Des.* **2019**, *19*, 4157-4161.

[12] a) Z. Zhang, J. Li, Y. Yao, S. Sun, *Cryst. Growth Des.* **2015**, *15*, 5028-5033; b) W. Yang, B. Li, H. Wang, O. Alduhaish, K. Alfooty, M. A. Zayed, P. Li, H. D. Arman, B. Chen, *Cryst. Growth Des.* **2015**, *15*, 2000-2004; c) W. Yang, F. Yang, T.-L. Hu, S. C. King, H. Wang, H. Wu, W. Zhou, J.-R. Li, H. D. Arman, B. Chen, *Cryst. Growth Des.* **2016**, *16*, 5831-5835; d) S. Roy, H. M. Titi, I. Goldberg, *CrystEngComm* **2016**, *18*, 3372-3382; e) Y.-H. Luo, X.-T. He, D.-L. Hong, C. Chen, F.-H. Chen, J. Jiao, L.-H. Zhai, L.-H. Guo, B.-W. Sun, *Adv. Funct. Mater.* **2018**, *28*, 1804822; f) X.-T. He, Y.-H. Luo, Z.-Y. Zheng, C. Wang, J.-

Y. Wang, D.-L. Hong, L.-H. Zhai, L.-H. Guo, B.-W. Sun, *ACS Applied Nano Materials* **2019**, *2*, 7719-7727; g) Y. Q. Li Yu-Ling, Liu Tian-Fu, Cao Rong, Yuan Wen-Bing, *Chinese J. Struct. Chem.* **2019**, *38*, 2083-2088; h) Y. Wang, D. Liu, J. Yin, Y. Shang, J. Du, Z. Kang, R. Wang, Y. Chen, D. Sun, J. Jiang, *Chem. Commun.* **2020**, *56*, 703-706; i) B. T. Liu, X. H. Pan, D. Y. Nie, X. J. Hu, E. P. Liu, T. F. Liu, *Adv. Mater.* **2020**, *32*, e2005912; j) Y. Wang, J. Yin, D. Liu, C. Gao, Z. Kang, R. Wang, D. Sun, J. Jiang, *J. Mater. Chem. A* **2021**, *9*, 2683-2688.

[13] a) G. R. Desiraju, *Angew. Chem. Int. Ed.* **1995**, *34*, 2311-2327; b) R. Chakrabarty, P. S. Mukherjee, P. J. Stang, *Chem. Rev.* **2011**, *111*, 6810-6918; c) A. Chaudhary, A. Mohammad, S. M. Mobin, *Cryst. Growth Des.* **2017**, *17*, 2893-2910; d) M. J. K. O. M. Yaghi, C. S. Diercks, *Introduction to Reticular Chemistry: Metal-Organic Frameworks and Covalent Organic Frameworks*, Wiley-VCH, Weinheim, **2019**; e) Y. Chen, X. Zhang, M. R. Mian, F. A. Son, K. Zhang, R. Cao, Z. Chen, S. J. Lee, K. B. Idrees, T. A. Goetjen, J. Lyu, P. Li, Q. Xia, Z. Li, J. T. Hupp, T. Islamoglu, A. Napolitano, G. W. Peterson, O. K. Farha, *J. Am. Chem. Soc.* **2020**, *142*, 21428-21438; f) G. Huang, L. Yang, Q. Yin, Z. B. Fang, X. J. Hu, A. A. Zhang, J. Jiang, T. F. Liu, R. Cao, *Angew. Chem. Int. Ed.* **2020**, *59*, 4385-4390; g) X.-J. Hu, Z.-X. Li, H. Xue, X. Huang, R. Cao, T.-F. Liu, *CCS Chem.* **2020**, *2*, 616-622.

[14] a) E. D. Stevens, *J. Am. Chem. Soc.* **1981**, *103*, 5087-5095; b) M.-S. Liao, S. Scheiner, *J. Chem. Phys.* **2002**, *117*, 205-219.

[15] G. R. Desiraju, *Crystal Design: Structure and Function*, Wiley-VCH, Weinheim, **2003**.

[16] a) T. S. Gautam R. Desiraju, *The Weak Hydrogen Bond, In Structural Chemistry and Biology*, Oxford University Press, USA, **2001**; b) T. Steiner, *Angew. Chem. Int. Ed.* **2002**, *41*, 48-76; c) I. A. Baburin, V. A. Blatov, L. Carlucci, G. Ciani, D. M. Proserpio, *CrystEngComm* **2008**, *10*, 1822-1838; d) B. C. Gibb, *Nat. Chem.* **2020**, *12*, 665-667.

[17] a) I. A. Baburin, V. A. Blatov, *Acta Crystallogr B* **2004**, *60*, 447-452; b) V. A. Blatov, A. P. Shevchenko, D. M. Proserpio, *Cryst. Growth Des.* **2014**, *14*, 3576-3586; c) V. A. Blatov *, *Crystallogr. Rev.* **2007**, *10*, 249-318.

[18] T. F. Willems, C. H. Rycroft, M. Kazi, J. C. Meza, M. Haranczyk, *Microporous Mesoporous Mater.* **2012**, *149*, 134-141.

[19] K. S. Walton, R. Q. Snurr, *J. Am. Chem. Soc.* **2007**, *129*, 8552-8556.

[20] a) J. B. Mann, T. L. Meek, L. C. Allen, *J. Am. Chem. Soc.* **2000**, *122*, 2780-2783; b) J. B. Mann, T. L. Meek, E. T. Knight, J. F. Capitani, L. C. Allen, *J. Am. Chem. Soc.* **2000**, *122*, 5132-5137.

[21] a) C. Mitterdorfer, M. Bauer, T. G. Youngs, D. T. Bowron, C. R. Hill, H. J. Fraser, J. L. Finney, T. Loerting, *Phys. Chem. Chem. Phys.* **2014**, *16*, 16013-16020; b) M. Schoen, C. L. Rhykerd, Jr., D. J. Diestler, J. H. Cushman, *Science* **1989**, *245*, 1223-1225; c) S. Cai, B. Sun, X. Li, Y. Yan, A. Navarro, A. Garzon-Ruiz, H. Mao, R. Chatterjee, J. Yano, C. Zhu, J. A. Reimer, S. Zheng, J. Fan, W. Zhang, Y. Liu, *ACS Appl. Mater. Interfaces* **2020**, *12*, 19054-19061.

[22] a) P. R. S. Salbego, C. R. Bender, N. Zanatta, C. P. Frizzo, H. G. Bonacorso, M. A. P. Martins, *ACS Omega* **2018**, *3*, 2569-2578; b) J. Hoja, H. Y. Ko, M. A. Neumann, R. Car, R. A. DiStasio, Jr., A. Tkatchenko, *Sci. Adv.* **2019**, *5*, eaau3338.

[23] G. W. T. M.J. Frisch, H.B. Schlegel, G.E. Scuseria, M.A. Robb, J.R. Cheeseman, G. Scalmani, V. Barone, G.A. Petersson, H. Nakatsuji, X. Li, M. Caricato, A.V. Marenich, J. Bloino, B.G. Janesko, R. Gomperts, B. Mennucci, H.P. Hratchian, J.V. Ortiz, A.F. Izmaylov, J.L. Sonnenberg, D. Williams-Young, F. Ding, F. Lipparini, F. Egidi, J. Goings, B. Peng, A. Petrone, T. Henderson, D. Ranasinghe, V.G. Zakrzewski, J. Gao, N. Rega, G. Zheng, W. Liang, M. Hada, M. Ehara, K. Toyota, R. Fukuda, J. Hasegawa, M. Ishida, T. Nakajima, Y. Honda, O. Kitao, H. Nakai, T. Vreven, K. Throssell, J.A. Montgomery Jr., J.E. Peralta, F.

7

Ogliaro, M.J. Bearpark, J.J. Heyd, E.N. Brothers, K.N. Kudin, V.N. Staroverov, T.A. Keith, R. Kobayashi, J. Normand, K. Raghavachari, A.P. Rendell, J.C. Burant, S.S. Iyengar, J. Tomasi, M. Cossi, J.M. Millam, M. Klene, C. Adamo, R. Cammi, J.W. Ochterski, R.L. Martin, K. Morokuma, O. Farkas, J.B. Foresman, D.J. Fox, Gaussian, Inc., Wallingford CT, **2009**.

[24]   S. P. Thomas, P. R. Spackman, D. Jayatilaka, M. A. Spackman, *J. Chem. Theory Comput.* **2018**, *14*, 1614-1623.

[25]   J. Contreras-Garcia, W. Yang, E. R. Johnson, *J. Phys. Chem. A* **2011**, *115*, 12983-12990.
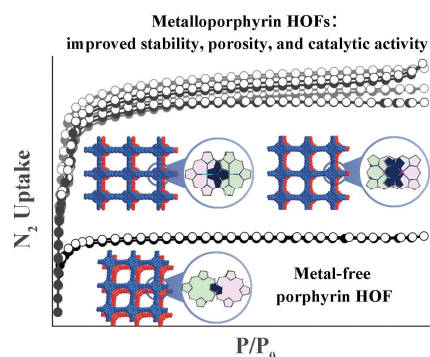
[26]   CCDC   2107777,   2107778,   2107780 contain the supplementary crystallographic data for this paper. These data can be obtained free of charge from the Cambridge Crystallographic   Data   Centre   via www.ccdc.cam.ac.uk/data_request/cif.

8

WILEY-VCH

Entry for the Table of Contents

Crystallographic and computational studies on a series of porphyrinic HOFs reveal that metallization of porphyrin centers greatly alters the orbital overlap of adjacent porphyrin, geometry of molecule/layer, and the strength of noncovalent interactions. Therefore, metalloporphyrin HOFs exhibit much higher stability, surface area, and catalytic activity than metal-free porphyrinic HOF.